SUPPORTING INFORMATION

Additive and interfacial control for efficient perovskite light-emitting diodes with reduced trap densities

Shun Tian, Chen Zou, Runchen Lai, Chungen Hsu, Xuhui Cao, Shiyu Xing, Baodan Zhao†, Dawei Di†

State Key Laboratory of Modern Optical Instrumentation, College of Optical Science and Engineering, International Research Center for Advanced Photonics, Zhejiang University, Hangzhou 310027, China

† Corresponding author E-mail: baodanzhao@zju.edu.cn (B.Z.); daweidi@zju.edu.cn (D.D.)

Materials and experimental methods

Materials. Cesium bromide (CsBr) (99.999%), Lithium fluoride (LiF) (99.99%, metal basis), Molybdenum oxide (MoO_x) (99.99%), Ag (99.999%) and Al (99.999%) were purchased from Alfa-Aesar. Lead bromide ($PbBr_2$) (99.999%), poly(9-vinylcarbazole) (PVK; molecular weight [MW] = 25,000-50,000 g mol^{-1}), and dimethyl sulfoxide (DMSO; 99.9%) were purchased from Sigma-Aldrich. Formamidinium bromide (FABr) (>99%), and 2',2'-(1,3,5-benzinetriyl)-Tris(1-phenyl-1-H-benzimidazole) (TPBi; > 98%) were purchased from Xi'an Polymer Light. 1,4,7,10,13,16-hexaoxacyclooctadecane (crown; 99%) was purchased from Acros. 2-(4-methoxyphenyl)ethylammonium bromide (MOPEABr) (>98%) were purchased from TCI. Nickel oxide (NiO_x) was purchased from Huamin (Beijing).

Sample preparation and device fabrication. Patterned ITO/glass substrates were washed by deionized water, acetone, isopropanol successively for average 30 min with sonication, and treated by UV-ozone for 30 minutes. NiO_x layers (20 mg mL^{-1}, dissolved in deionized water) and PVK layers (dissolved in chlorobenzene; 6 mg mL^{-1}) were spin-coated on ITO/glass substrates at 4,000 rpm and 4,500 rpm, sequentially, followed by annealing at 150℃ for 30 minutes. 1-nm LiF was evaporated onto PVK. The $(MOPEA)_2(Cs_xFA_{1-x})_{n-1}Pb_nBr_{3n+1}$ (MCFPB) perovskite precursor was prepared by dissolving 28 mg MOPEABr, 64 mg CsBr, 7.5 mg FABr, 110 mg $PbBr_2$ in 1 mL DMSO. The $(MOPEA)_2(Cs_xFA_{1-x})_{n-1}Pb_nBr_{3n+1}$-crown (MCFPB-C) precursor was prepared by adding 4 mg crown into 1 mL MCFPB precursor. The MCFPB or MCFPB-C precursors were spin-coated onto the hole transport layers (NiO_x/PVK/LiF) at 4,000 rpm, annealed at 70℃ for 5 minutes. Finally, TPBi (~45 nm), LiF (1 nm), and Al (~100 nm) electrodes

were sequentially evaporated through a shadow mask (active pixel area = 3.5 mm^2) at a pressure of 10^{-6} mbar. The devices were encapsulated with UV epoxy (NOA81, Thorlabs)/coverglass to minimize exposure to oxygen and moisture during measurements.

Material and device characterization. Current density (J)-voltage (V)-Luminance (L) characteristics were measured using a Keithley 2400 source-meter unit. The EQEs of the devices were calculated based on the luminance data and a Lambertian emission profile. The transient PL decay was measured using a time-correlated single-photon counting (TCSPC) setup (Horiba DeltaFlex). Transient absorption measurements were carried out using an Ultrafast Systems LLC pump-probe system. The surface morphologies of the perovskite films were characterized by scanning-electron microscopy (SEM, HITACHI, SU-70) and atomic force microscopy (AFM, VEECO Multimode), respectively. A UV-vis spectrophotometer (UV1901) was used to measure the absorption spectrum. The UV photoelectron spectroscopy (UPS) spectra were measured using a Thermo Scientific ESCALAB 250Xi with excitation provided by the He I emission line (21.2 eV) of a helium discharge lamp. The work functions of the samples were calculated using $\Phi = 21.2\text{-}E_{cutoff}$. The valence band maximum (VBM) was determined by the linear extrapolation of the leading edge of the valence band to zero baseline intensity. The bandgap values ($E_{bandgap}$) were derived from the UV-vis absorption spectra[1]. The energy position of conduction band minimum (CBM) was calculated by the equation $E_{CBM} = E_{VBM} + E_{bandgap}$. The X-ray diffraction (XRD) measurements were carried out on perovskite films on quartz substrates using a Ultima IV with Cu Kα1.2 radiation (λ = 0.15418 nm). The spectra were collected within an angular range of 5º-55º with a scanning speed of 2º/min. The cross-sectional transmission electron microscopy (TEM) image of the device structure was obtained by a Cs aberration-corrected Titan microscope at 200 kV (G2 80-200, with ChemiSTEM technology).

Optical simulation of PeLEDs. The dipole orientation of emitters is assumed to be isotropic. The refractive indices (n) and extinction coefficients (k) of each layer in the PeLEDs were determined by ellipsometry. The refractive index of the MCFPB-C layer is 1.9 at 511 nm. Fig. 2(e) shows the optical power distribution of PeLEDs with isotropic dipole orientation. Different optical channels are present in the PeLEDs[2, 3]: direct emission, substrate mode, waveguide mode, and surface plasmon mode. Fig. 2(f) illustrated the simulation of power distribution into the optical modes of PeLEDs with different perovskite layer thicknesses for isotropic dipole orientation with the assumption of γ = 1 and η_{e-h} = 1. Variation of the perovskite layer thickness significantly alters the fraction of outcoupled light through modifying the PeLED cavity length[2-4]. The losses through surface plasmons are primarily determined by the distance between the emissive dipole and the metallic electrode. Consequently, increasing the perovskite layer thickness can reduce the fraction of surface plasmon mode. However, the reduced surface plasmon mode mostly coupled to the waveguide

mode. The four channels were divided by the in-plane wavevector k_{xy}. Details are described as follows[2, 3]: (1) Direct emission: $k_0 \cdot n_{air} \geq k_{xy} \geq 0$, where $k_0 = 2\pi/\lambda$ is the vacuum wave vector and n_{air} is the refractive index of air. (2) Substrate mode: $k_0 \cdot n_{sub} \geq k_{xy} > k_0 \cdot n_{air}$, where n_{sub} is the refractive index of glass substrate. Photons experience the total internal reflection at the air/substrate interface and are trapped inside the glass substrate. (3) Waveguide mode: $k_0 \cdot n_{eff} \geq k_{xy} > k_0 \cdot n_{sub}$, where n_{eff} is the real part of the equivalent refractive indices of the charge transport layers, the perovskite layer and the ITO layer (the metallic electrode layer is not included). Light is trapped inside the functional layer stack between the top-surface of the glass substrate and aluminum electrode. (4) Surface plasmon: $k_{xy} > k_0 \cdot n_{eff}$, this mode corresponds to evanescent waves at the electron-transport layer (TPBi)/the metal interface. A large amount of light coupled to one weak and one sharp waveguide mode (region 3) and one surface plasmon mode (region 4).

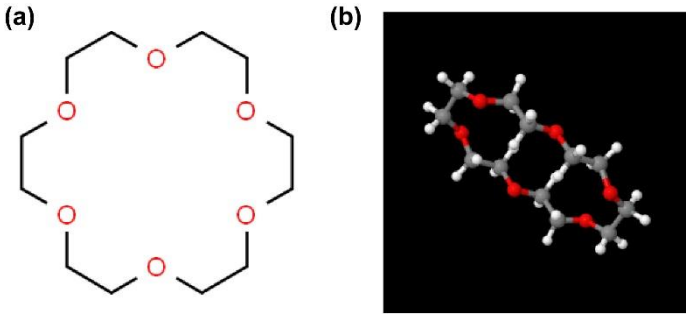

Fig. S1. Chemical structure of crown in (a) 2D and (b) 3D.

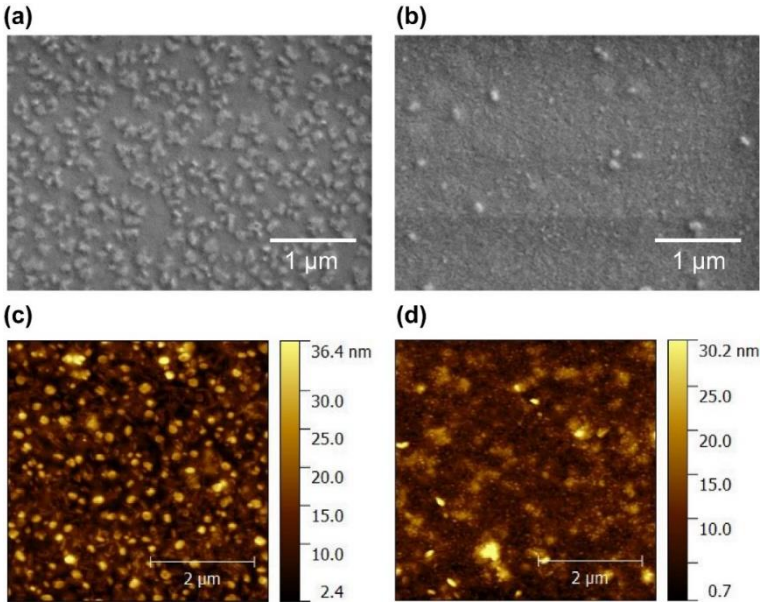

Fig. S2. Morphological characterization of MCFPB and MCFPB-C perovskite films on quartz substrates. SEM images of (a) MCFPB sample and (b) MCFPB-C sample. AFM images of (c) MCFPB sample and (d) MCFPB-C sample.

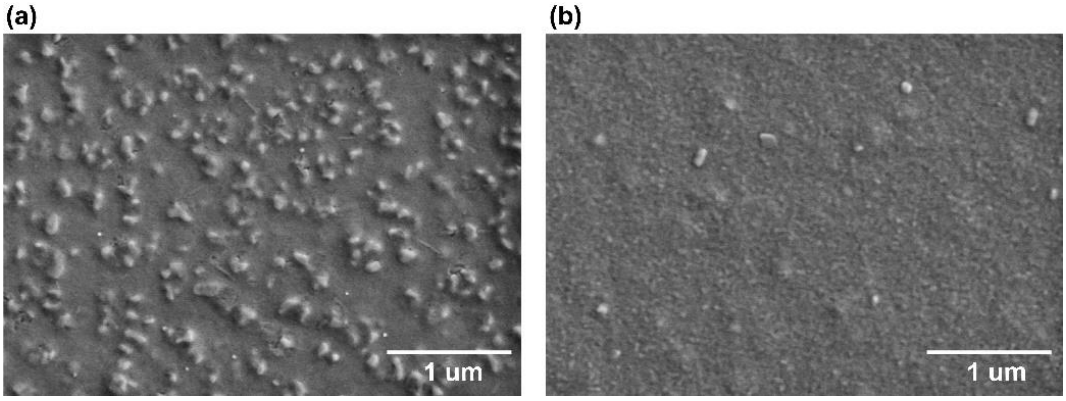

Fig. S3. The SEM images of (a) MCFPB and (b) MCFPB-C films on LiF (1 nm)-coated quartz substrates.

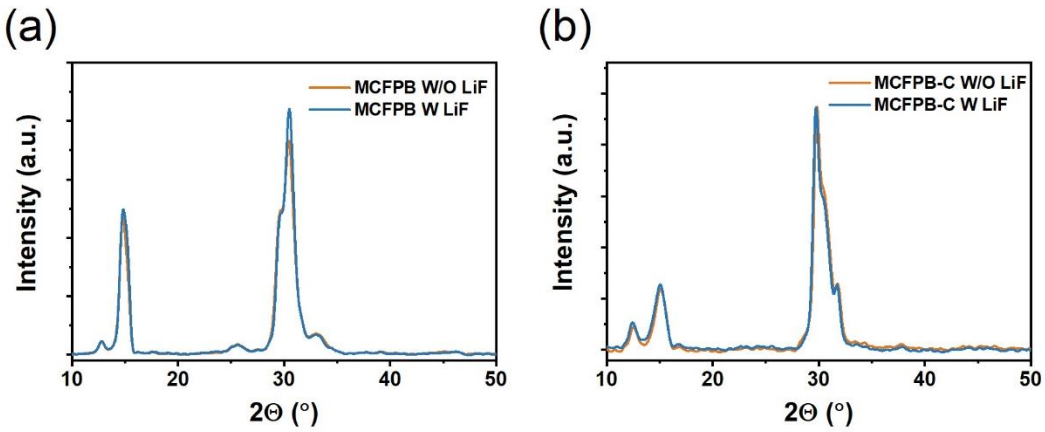

Fig. S4. The XRD patterns of (a) MCFPB and (b) MCFPB-C films on quartz and LiF (1 nm)-coated quartz substrates.

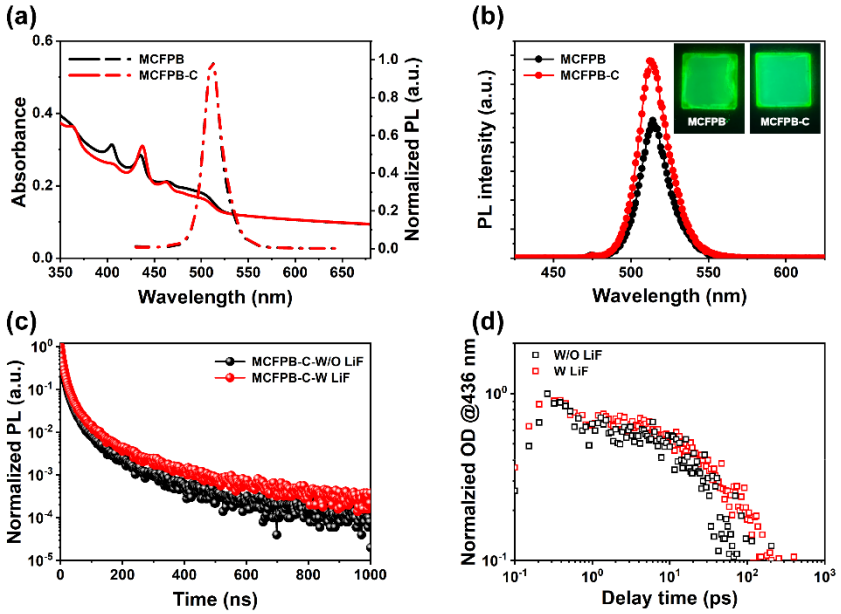

Fig. S5. Optical characteristics of MCFPB and MCFPB-C perovskite films. (a) Absorption spectra and normalized PL spectra of MCFPB and MCFPB-C films. (b) PL intensity of MCFPB and MCFPB-C on quartz substrates. Insets: images of MCFPB and MCFPB-C samples under UV lamp. (c) Time-resolved PL decay and (d) TA kinetics traces probed at 436 nm of MCFPB-C on bare quartz or quartz/LiF substrates.

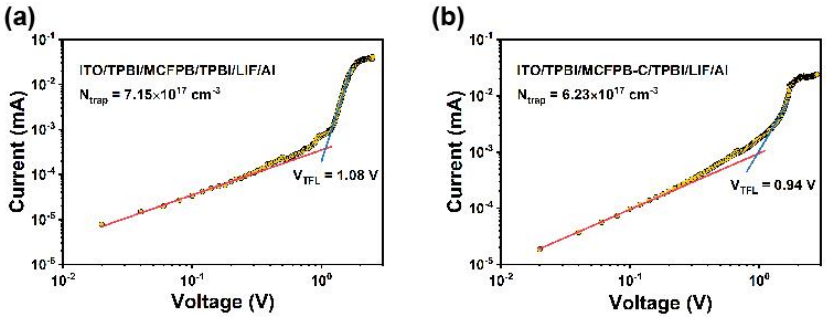

Fig. S6. SCLC analyses for MCFPB and MCFPB-C perovskite films. Current-voltage characteristics of devices with structures of (a) ITO/TPBi/MCFPB/TPBi/LiF/Al, (b) ITO/TPBi/MCFPB-C/TPBi/LiF/Al.

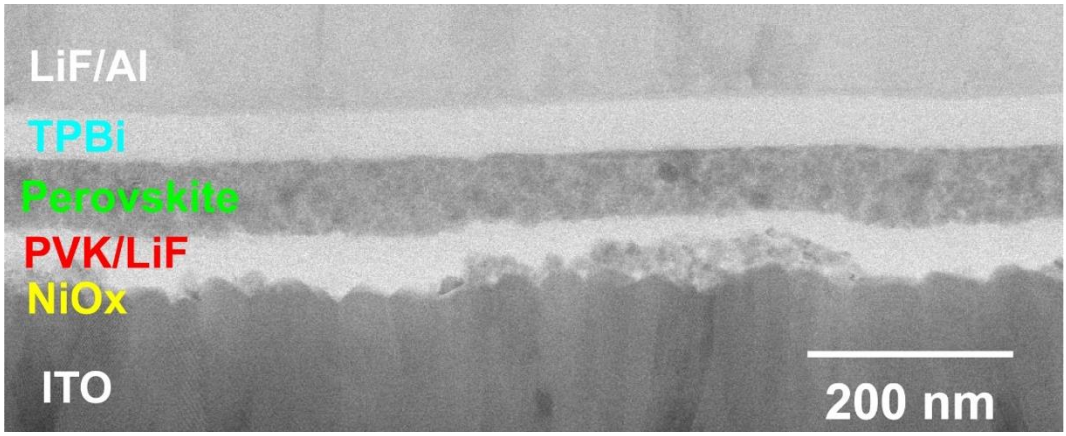

Fig. S7. Cross-sectional TEM image of a PeLED based on MCFPB-C perovskite.

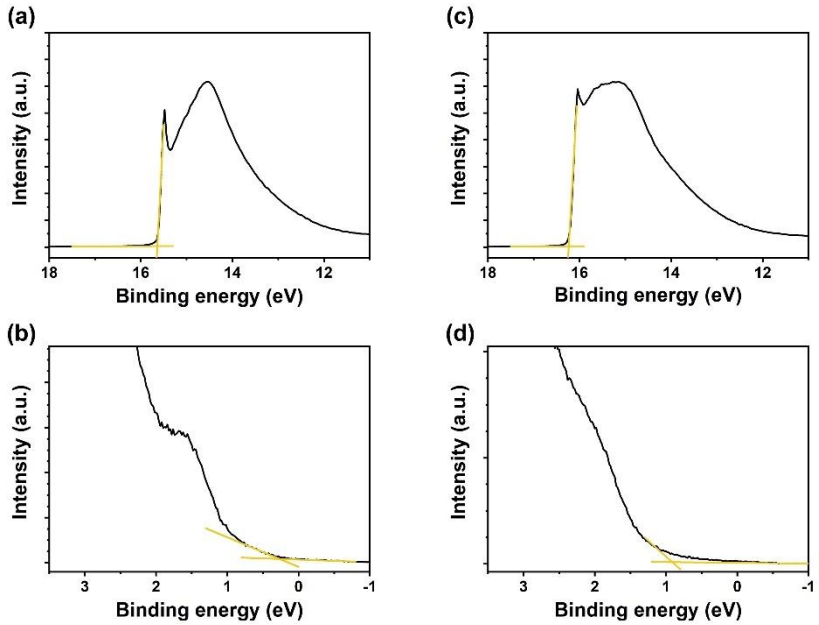

Fig. S8. UPS and valence band spectra of different perovskite samples. (a, b) MCFPB; (c, d) MCFPB-C.

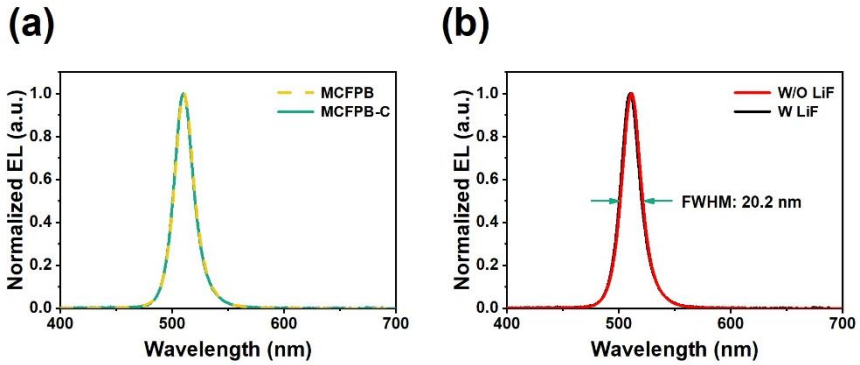

Fig. S9. (a) The EL spectra of devices based on (a) MCFPB and MCFPB-C films, (b) MCFPB-C with and without LiF interface.

Table S1. The energy levels of perovskite films determined from the UPS spectra.

Perovskite film	E_{cutoff} (eV)	Work function (eV)	Valence band maximum (eV)	Conduction band minimum (eV)
MCFPB	15.6	5.6	-3.5	-5.8
MCFPB-C	16.2	5.0	-3.6	-5.9

References

[1] Yao D, Zhang C, Pham N D, et al. Hindered formation of photoinactive δ-$FAPbI_3$ phase and hysteresis-free mixed-cation planar heterojunction perovskite solar cells with enhanced efficiency via potassium incorporation. J Phys Chem Lett, 2018, 9, 2113

[2] Zou C, Lin L. Effect of emitter orientation on the outcoupling efficiency of perovskite light-emitting diodes. Opt Lett, 2020, 45

[3] Zhu R, Luo Z, Wu S. Light extraction analysis and enhancement in a quantum dot light emitting diode. Opt Express, 2014, 22 Suppl 7, A1783

[4] Zhao L, Lee K M, Roh K, et al. Improved outcoupling efficiency and stability of perovskite light-emitting diodes using thin emitting layers. Adv Mater, 2019, 31, e1805836